International Journal of Thermal Sciences 111 (2017) 289–300

Contents lists available at ScienceDirect

International Journal of Thermal Sciences

journal homepage: www.elsevier.com/locate/ijts

Turbulent flow and heat transfer enhancement in a heat exchanger tube fitted with novel discrete inclined grooves

Nianben Zheng*, Peng Liu, Feng Shan, Zhichun Liu, Wei Liu**

School of Energy and Power Engineering, Huazhong University of Science and Technology, Wuhan 430074, China

ARTICLE INFO

Article history:
Received 21 October 2015
Received in revised form
9 September 2016
Accepted 11 September 2016

Keywords:
Discrete inclined groove
Heat transfer enhancement
Entropy generation

ABSTRACT

In the present work, we propose a novel enhanced tube with discrete inclined grooves, aiming to enhance heat transfer with minimum consumption of pump power by generating longitudinal swirl flows with multiple vortices in the proposed grooved tube. A numerical study has been conducted to investigate the turbulent flow structures and the effects of geometric parameters on the thermal performance. According to the results, longitudinal swirl flows with multiple vortices are generated in the grooved tube, and the number of induced vortices is proportional to the number of circumferential grooves. The heat transfer and friction factor are enhanced by a factor of approximately 1.23–2.17 and 1.02 to 3.75 over the smooth tube, respectively. To further understand the physical mechanism of the enhanced grooved tube and to assess the effects of geometric parameters, entropy generation analyses have also been performed. The results show that the entropy generation number ratios decrease with increasing the number of circumferential grooves and with the reduced groove pitch ratio, and a number of circumferential grooves of 12 and a groove pitch ratio of 3 are recommended for the proposed grooved tube. In addition, comparisons with previous work show that the proposed grooved tube provides considerably higher overall thermal performance than the transversally grooved tube, internally helical grooved tube and continuous corrugated tube, but lower thermal performance than the discrete corrugated tube at lower Reynolds numbers, indicating that the proposed grooved tube is very promising for heat transfer enhancement in practical applications.

1. Introduction

Heat exchangers, which ensure heat transfer from one medium to another, have wide applications ranging from petroleum, chemical, power generation industries and domestic uses. Enhancement in a heat exchanger's overall performance contributes to reducing the size of heat exchangers and make material and energy savings related to the heat exchange processes [1]. In practical applications, it is usually necessary to develop efficient enhanced heat transfer tubes to improve the efficiency of a heat exchanger, due to the fact that a heat exchanger's overall performance is determined by the heat transfer in the tubes which are the basic heat transfer units for a heat exchanger. Tube inserts like twisted tapes and coiled wires or artificial roughness elements such as ribs, grooves and corrugations on the surface are commonly used heat transfer enhancement techniques for tubes. Among these techniques available, artificial grooved tubes show better overall thermal performance and are widely used in modern heat exchangers, because they are very effective in heat transfer augmentation [2].

Bilen et al. [2] experimentally investigated the effects of groove geometry on heat transfer for internally grooved tube. Three geometric groove shapes (circular, trapezoidal, and rectangle) were adopted to perform the tests. The heat transfer enhancement was obtained up to 63% for circular groove, 58% for trapezoidal groove and 47% for rectangle groove, compared to the smooth tube. Aroonrat et al. [3] studied the heat transfer and flow characteristics of water flowing through horizontal internally grooved tubes, including one straight grooved tube and four helical grooved tubes with different pitches. The results showed that the thermal enhancement factor obtained from helical grooved tubes is about 1.4–2.2 for a pitch of 0.5 inch; 1.1 to 1.3 for pitches of 8, 10, and 12 inches, respectively; and 0.8 to 0.9 for a straight grooved tube. Bharadwaj et al. [4] determined pressure drop and heat transfer characteristics of flow of water in a 75-start spirally grooved tube

* Corresponding author.
** Corresponding author.
E-mail addresses: ben@hust.edu.cn (N. Zheng), w_liu@hust.edu.cn (W. Liu).

http://dx.doi.org/10.1016/j.ijthermalsci.2016.09.010
1290-0729/

with twisted tape insert experimentally. Laminar to fully turbulent ranges of Reynolds numbers were considered in the experiments. It was found that heat transfer enhancement due to spiral grooves was further augmented by inserting twisted tapes compared to smooth tube.

Experimental measurements and analyses about transition and turbulent convective heat transfer performances of molten salt in the spirally grooved tube were conducted by Lu et al. [5]. According to the experimental results, the groove height increment remarkably enhanced heat transfer in the spirally grooved tube. Later, Lu et al. [6] experimentally investigated the convective heat transfer of high temperature molten salt in transversely grooved tube using electric power through the testing tube, and developed experimental correlation for molten salt flow in transversely grooved by considering the groove height.

There are further studies concerning the thermal-hydraulic performance for condensation and evaporation in the grooved tubes. Goto et al. [7] measured heat transfer coefficient and pressure drop for condensation and evaporation of R410A and HCFC22 inside conventional spiral groove tubes and herring-born groove tubes. The results showed that the local heat transfer coefficients of the herring-bone grooved tubes were about twice as large as those of spiral one for condensation, and were slightly larger than those of spiral one for the evaporation. Zhang et al. [8,9] carried out experimental studies on heat transfer characteristics for evaporation of R417A flowing inside horizontal smooth and internally grooved tubes. Recently, Zhang et al. [10] investigated heat transfer enhancement and pressure drop performance for R417A flow boiling in smooth and internally grooved tubes experimentally. The results indicated that both enhancement factor and penalty factor increased with increasing mass flux, while enhancement parameters showed different situations in different internally grooved tubes.

Grooves have also been applied in other channels besides circular tubes. A numerical investigation of turbulent forced convection in a two-dimensional channel with periodic transverse grooves on the lower channel wall was conducted by Eiamsa-ard and Promvonge [11]. Latser, they [12] experimentally examined the turbulent forced convection heat transfer and friction characteristics in a rectangular duct with rib-grooved turbulators. Bi et al. [13] examined the local heat transfer characteristics in the mini-channels with enhanced dimples, cylindrical grooves and low fins by using the field synergy principle. Liu et al. [14] proposed novel groove geometries, which were conventional cylindrical grooves with rounded transitions to the adjacent flat surfaces and with modifications to their bases, and numerically analyzed the turbulent flow characteristics and heat transfer performances in square channels with different cylindrical-shaped grooves. According to the numerical results, the rounded transition of the grooves had a large advantage over conventional cylindrical grooved surfaces in both enhancing heat transfer and reducing pressure loss penalty. Tang et al. [15] numerically investigated the effects of groove configurations and various geometric parameters on heat transfer enhancement in a narrow channel with discrete grooved structures. The results of parameters study showed that the case of P-type grooves with $p_h = 1.2, f_h = 2.6, e_h = 1, \alpha = 30^\circ$ provided the best overall thermal performance factor at $Re = 4016$.

According to the above literature survey, grooves can be used to improve thermal performance for single-phase flow or two-phase flow in circular tubes or other channels. However, utilizations of the grooves usually result in a considerable increase in the pressure drop for the heat transfer enhancement. To provide guidelines for achieving energy savings by improving the balance between heat transfer enhancement and pressure drop, our group has carried out several heat transfer optimization studies [16–20]. The theoretical results obtained show that longitudinal swirl flow with multiple vortices is a flow pattern that can lead to high overall thermal performance of circular tubes.

In Ref. [21], Meng proposed a double discrete inclined ribbed tube (DDIR-tube) for heat transfer enhancement. The results show that longitudinal swirl flows with multiple vortices can be generated with the unique arrangement of the ribs. In the present work, we propose a novel enhanced tube with discrete inclined grooves. The arrangement and size of grooves are similar to those of ribs as shown Ref. [21]. The objective of this work is aiming to enhance heat transfer with minimum consumption of pump power by generating longitudinal swirl flows with multiple vortices in the proposed grooved tube. A numerical study of turbulent flow and heat transfer in the grooved tube is conducted to document the possibilities. Turbulent flow and heat transfer details, and effects of geometric parameters on the flow and heat transfer are presented and analyzed. To understand the physical mechanism of the enhanced grooved tube and to assess the effects of geometric parameters on the heat transfer performance, entropy generation analyses have also been performed to further reveal the essence of heat transfer enhancement.

2. Model description

The schematic diagram of the circular tube with discrete grooves characterized by a discrete and inclined distribution investigated in the present numerical work is shown in Fig. 1. The tube consisted of three sections with a total length of 0.4 m (l). The test section had a length of 0.2 m (L_2), an inner diameter (D_1) of 0.017 m and an outer diameter (D_2) of 0.019 m. To guarantee a nearly fully developed flow situation and to eliminate downstream disturbance effects; two extended smooth tubes with lengths of $10D_1$ (L_1) and $10D_1$ (L_3) were connected upstream and downstream of the test section, respectively.

In the test section, discrete inclined grooves were uniformly arranged on the inner wall surface of the tube as shown in Fig. 2. The fixed geometric parameters for the grooves were groove length (L = 0.006 m), groove width (W = 0.002 m), groove depth (H = 0.0005 m) and groove inclination angle ($\alpha = 30^\circ$). Five values of the number of circumferential grooves (N = 4, 6, 8, 10, 12); and five values of the groove pitch ratio, defined as the ratio of the groove pitch to the groove width ($P^* = P/W = 3, 4, 5, 6, 7$) were used to examine the influence of geometric parameters on heat transfer and flow performance in the grooved tube.

3. Numerical simulations

3.1. Selection of turbulence model

The selection of an appropriate turbulence model is crucial to the accuracy of numerical results. The commonly used turbulence models in engineering applications, including the *realizable* k-ε Model, the *standard* k-ω Model and the *SST* k-ω Model were used to investigate the steady-state, three-dimensional turbulent flow and heat transfer characteristics of the DDIR-tube as documented in Ref. [21]. The results obtained using these turbulent models were compared with the experimental data, as shown in Fig. 3. It is evident that the average Nusselt number calculated by the *SST* k-ω Model is most similar to the experimental data of the model tested than that using other turbulence models. Quantitatively, the maximum deviations for the average Nusselt number between the experimental and numerical data for the *realizable* k-ε Model, the *standard* k-ω Model and the *SST* k-ω Model are 9.4%, 8.4% and 6%, respectively, indicating that the *SST* k-ω Model is more reliable than other models. Therefore, the *SST* k-ω Model was employed for

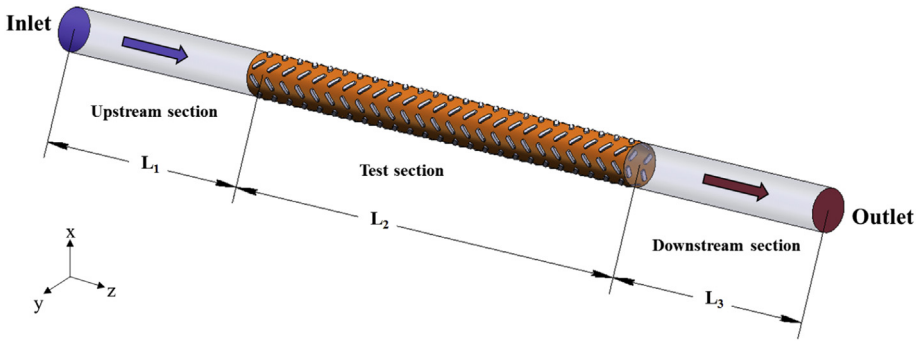

Fig. 1. Schematic diagram of the grooved tube.

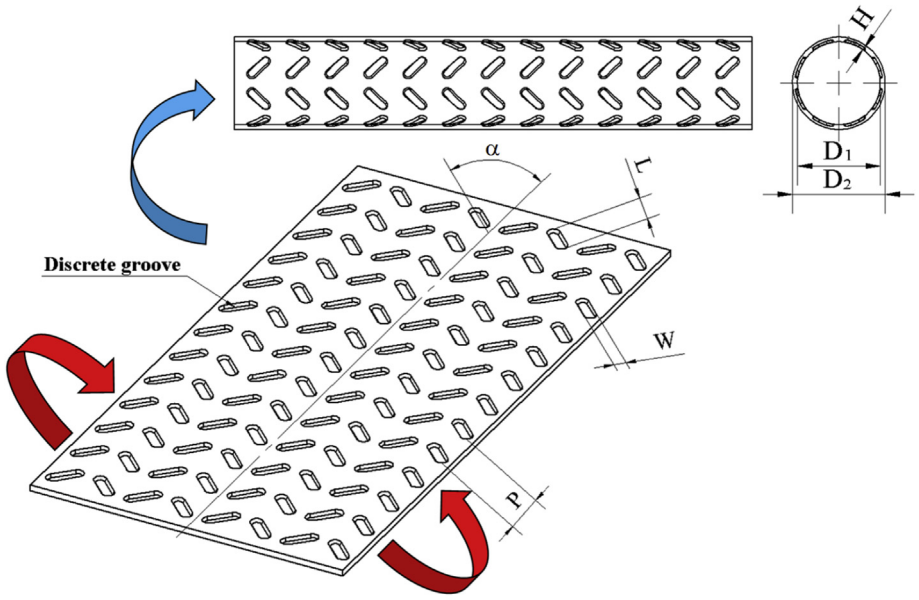

Fig. 2. Structure and configurations of the discrete inclined grooves.

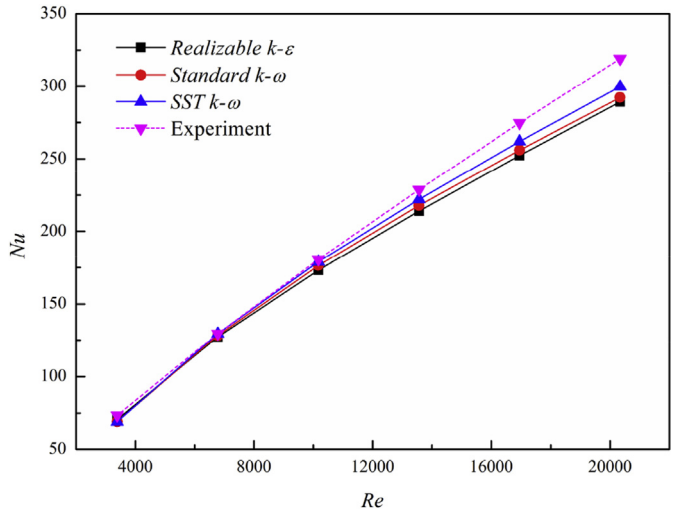

Fig. 3. Validation of turbulence models by comparing numerical and experimental average Nusselt number in the ribbed tube [21] using three turbulence models.

further numerical investigations in the present study.

3.2. Governing equations and boundary conditions

The flow field is governed by the three-dimensional Reynolds-averaged Navier–Stokes (RANS) equations, based on the assumption that the heat transfer and fluid flow processes are turbulent and steady-state, and that heat loss to the environment is neglected. The governing equations are as follows [22]:

Continuity equation:

$$\frac{\partial(\rho u_i)}{\partial x_i} = 0 \tag{1}$$

Momentum equation:

$$\frac{\partial(\rho u_i)}{\partial t} + \frac{\partial(\rho u_i u_j)}{\partial x_j} = -\frac{\partial p}{\partial x_i} + \frac{\partial}{\partial x_j}\left[\mu\frac{\partial(u_i)}{\partial x_j} - \rho\overline{u_i' u_j'}\right] \tag{2}$$

Energy equation:

$$\frac{\partial}{\partial x_i}(\rho T) + \frac{\partial}{\partial x_i}(\rho u_i T) = \frac{\partial}{\partial x_i}\left[\frac{\lambda}{c_p}\frac{\partial T}{\partial x_i}\right] \tag{3}$$

The turbulence kinetic energy equation:

$$\frac{\partial(\rho k)}{\partial t}+\frac{\partial(\rho u_i k)}{\partial x_i}=\tilde{P}_k-\beta^*\rho k\omega+\frac{\partial}{\partial x_i}\left[(\mu+\sigma_k u_t)\frac{\partial k}{\partial x_i}\right] \tag{4}$$

The specific dissipation rate equation:

$$\frac{\partial(\rho\omega)}{\partial t}+\frac{\partial(\rho u_i\omega)}{\partial x_i}=\varphi\rho S^2-\beta\rho\omega^2+\frac{\partial}{\partial x_i}\left[(\mu+\sigma_\omega\mu_t)\frac{\partial\omega}{\partial x_i}\right]+2(1-F_1)\rho\sigma_{w2}\frac{1}{\omega}\frac{\partial k}{\partial x_i}\frac{\partial\omega}{\partial x_i} \tag{5}$$

where the blending function F_1 is defined by:

$$F_1=\tanh\left[\left[\min\left[\max\left[\frac{\sqrt{k}}{\beta^*\omega y},\frac{500\nu}{y^2\omega}\right],\frac{4\rho\sigma_{\omega2}k}{CD_{k\omega}y^2}\right]\right]^4\right] \tag{6}$$

where $CD_{k\omega}=\max\left[2\rho\sigma_{\omega2}\frac{1}{\omega}\frac{\partial k}{\partial x_i}\frac{\partial\omega}{\partial x_i},10^{-10}\right]$ and y is the distance to the nearest wall.

The turbulent eddy viscosity is defined as follows:

$$\nu_t=\frac{\varphi_1 k}{\max(\varphi_1\omega,SF_2)} \tag{7}$$

where S is the invariant measure of the strain rate and F_2 is a second blending function defined by:

$$F_2=\tanh\left[\left[\max\left[\frac{2\sqrt{k}}{\beta^*\omega y},\frac{500\nu}{y^2\omega}\right]\right]^2\right] \tag{8}$$

A production limiter is used in the *SST* model to prevent the build-up of turbulence in stagnation regions:

$$P_k=\mu_t\frac{\partial u_i}{\partial x_j}\left[\frac{\partial u_i}{\partial x_j}+\frac{\partial u_j}{\partial x_i}\right]\rightarrow\tilde{P}_k=\min\left(P_k,10\cdot\beta^*\rho k\omega\right) \tag{9}$$

All constants are computed by a combination of the corresponding constants of the $k-\varepsilon$ and $k-\omega$ models via $\varphi=\varphi_1F+\varphi_2(1-F)$, etc. The constants for this model are as follows: $\beta^*=0.09$, $\varphi_1=5/9$, $\beta_1=3/40$, $\sigma_{k1}=0.85$, $\sigma_{\omega1}=0.5$, $\varphi_2=0.44$, $\beta_2=0.0828$, $\sigma_{k2}=1$, $\sigma_{\omega2}=0.856$ All the governing equations were solved using the Fluent 13.0 software, which is based on the finite volume method. The SIMPLE algorithm was used for the velocity–pressure coupling, and the second-order upwind scheme was applied for the discretization of the convection terms. The diffusion terms were discretized using a central difference scheme. The minimum convergence criterion was 10^{-6} for the continuity equation, velocity and turbulence quantities and 10^{-8} for the energy equation.

For a full length grooved tube, a uniform velocity was introduced at the inlet and the fluid temperature of the inlet was fixed at 293 K, while a pressure-outlet condition was applied at the outlet. Non-slip velocity conditions on the walls were assumed. A constant and uniform temperature of 333 K was applied on all walls. Water was selected as the working fluid, and all results were obtained under steady-flow conditions with Reynolds numbers ranging from 6780 to 20340.

3.3. Grid generation and independence test

The fluid domain was discretized by unstructured mesh generated with the commercial software ICEM CFD 13.0 as shown in Fig. 4. To obtain more precise results and ensure that y^+ remained less than 1, prism grids, which are orthogonal to the surfaces and with faces perpendicular to the boundary layer flow direction, were extruded from the surface of the tube. A hex core mesh, with hexahedron grids filling the majority of the volume, was generated to capture the characteristics of the fluid flow in the core region. To fill the areas between the surface of the prisms and the hex core, tetrahedron grids were used. Pyramids were applied to establish a conformal connection between triangle and quadrangle faces. To confirm the accuracy of the numerical solutions, three sets of grid systems, with 5171256, 6477267 and 8531495 elements, were used in a simulation to perform a grid independence test at a Reynolds number of 10170. The *Nu* and *f* values obtained by the three grid systems are illustrated in Fig. 5. The results indicate that the deviation between the calculated values for grids comprising 6477267 and 8531495 elements is about 0.9% for Nusselt number and 1.2% for friction factor, indicating that the grid system with 6477267 elements is adequately dense for the simulations. Therefore, this grid system with 6477267 elements was adopted in the subsequent simulation reflecting a compromise of computational time and solution precision.

3.4. Parameter definition

The Reynolds number (Re) is given by

$$Re=\frac{\rho u_m D_1}{\mu} \tag{10}$$

where u_m is the mean velocity in the tube.

The average heat transfer coefficient (h) and the Nusselt number (Nu) are estimated as follows:

$$h=\frac{q}{T_w-T_m} \tag{11}$$

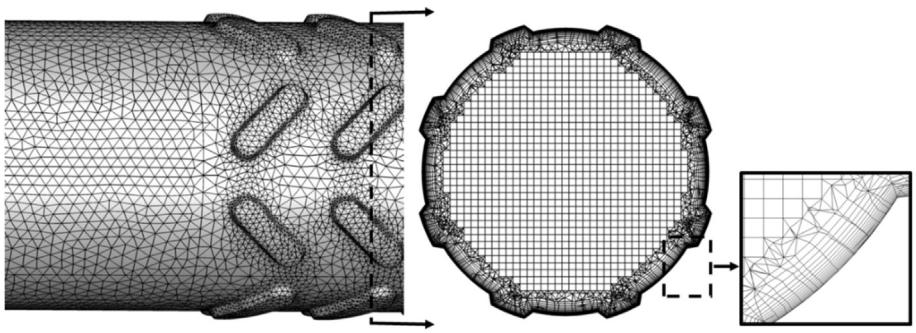

Fig. 4. Grids generated for the computation domain.

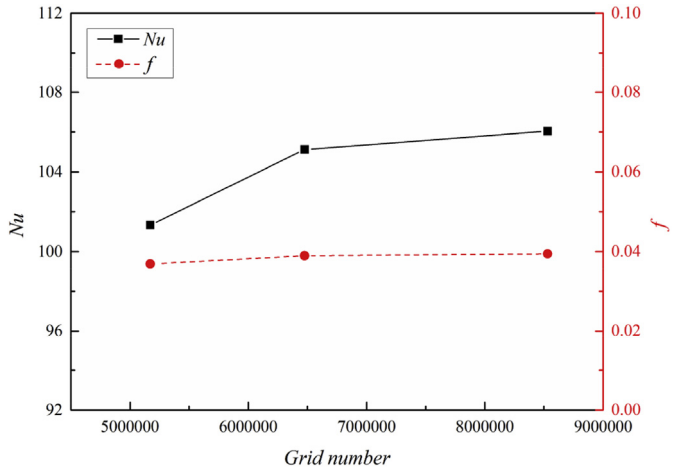

Fig. 5. Nusselt number and friction factor calculated by different grid systems at $Re = 10170$.

$$Nu = \frac{hD_1}{k} \tag{12}$$

where T_w is the average temperature of the wall and T_m is the bulk temperature of the fluid.

Correspondingly, the friction factor (f) can be written as

$$f = \frac{\Delta P}{(L_2/D_1)\rho u_m^2/2} \tag{13}$$

in which ΔP could be determined by the difference between the mass-averaged pressures at the inlet and the outlet of the test section.

To evaluate more real benefits with the application of present grooved tubes, the more realistic ratio $Q_{*,b}$ proposed by Bergles et al. [23,24] is computed. Real benefits can be obtained when the ratio is more than one. It is calculated based on the following formula:

$$Q_{*,b} = Q_a^{'} \Big/ Q_s^{'} \tag{14}$$

where $Q_a^{'}$ and $Q_s^{'}$ are the total heat flux transferred in the enhanced tube and smooth tube, respectively.

4. Results and discussion

4.1. Code validation

To test the reliability of the numerical methods and procedures adopted in this study, the numerical results obtained for turbulent flow in a smooth tube were compared to the data obtained by the standard correlations. This kind of approach to code validation has often been adopted for numerical investigations when experimental data is insufficient or unavailable in the open literature. The standard correlations for Nusselt number and friction factor for a turbulent flow through the smooth tube are correlation of Gnielinski [25] and correlation of Petukhov [26], respectively.

Correlation of Gnielinski is given by

$$Nu_0 = \frac{(\zeta/8)(\mathrm{Re} - 1000)\mathrm{Pr}}{1 + 12.7\sqrt{\zeta/8}(\mathrm{Pr}^{2/3} - 1)} \tag{15}$$

$$\zeta = (1.821\mathrm{g}\ \mathrm{Re} - 1.64)^{-2} \tag{16}$$

Correlation of Petukhov is expressed as

$$f_0 = (0.79\ \ln \mathrm{Re} - 1.64)^{-2} \tag{17}$$

Comparisons between numerical results and correlations are shown in Fig. 6. The results obtained for the smooth tube from the numerical simulations are found to agree well with those from the correlations, within 4.6% and 1.2% for the Nusselt number and friction factor, respectively. Therefore, numerical methods adopted in this study for heat transfer and pressure drop predictions were judged to be reliable.

4.2. Flow structure and temperature distributions

Prior to investigating the effects of geometric parameters on the thermal-hydraulic performance in the tube with discrete inclined grooves, it is necessary to analyze the flow structure and temperature distributions in the grooved tube at first. The flow structure inside grooves of the proposed enhanced tube is visualized in Fig. 7. It is evident from the streamlines inside the groove that swirl flows are induced inside the grooves as the incoming flows swallowed into the grooves. A closer examination of the streamlines shows

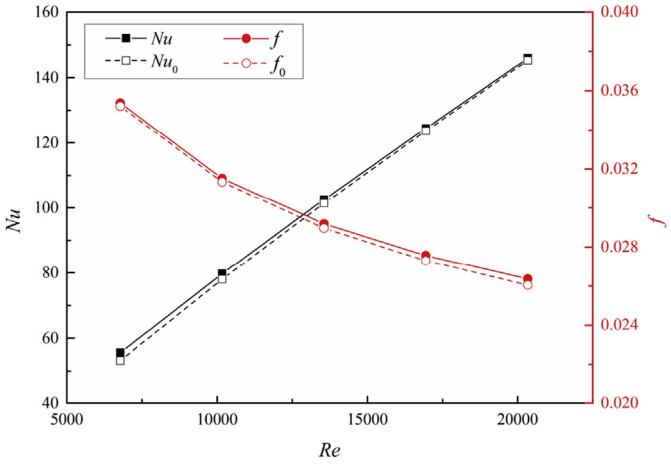

Fig. 6. Validation of Nusselt number and friction factor for the smooth tube.

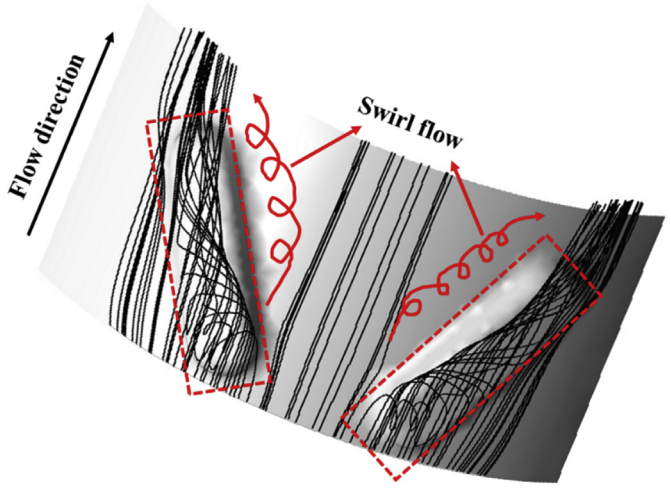

Fig. 7. Streamlines inside grooves.

that flow separation occurs closer to the rear edge side of the groove, and separated flows will reattach closer to the front edge side of the groove. After recirculation inside the groove, the swirl flows are injected from the grooves. Apparently, swirl flow, flow deviation and redirection are the main features of the flow structure in the proposed grooved tube.

Fig. 8 shows the tangential velocity vectors and temperature contours in the outlet cross section of the test section which are the most notable characteristics of the effects of the discrete inclined grooves on the mainstream flow and heat transfer. It is visible that three pairs of counter-rotating vortices or longitudinal swirl flows near the wall are generated inside the grooved tube. Each longitudinal swirl flow is induced as the incoming flows pass over a discrete inclined groove, and the mainstream is finally divided into six helical streams. The flow pattern results in a long flow path and relatively intense flow mixing between the wall and the core flow regions, which affects the temperature distributions in the grooved tube significantly. A closer inspection of the temperature contours shows that larger temperature gradients are created where the cold fluids swallowed from the core flow region impinge toward the tube wall, while in the regions where hot fluids near the wall flow toward the core flow region, the temperature gradients are relatively smaller. On the whole, the temperature is more evenly distributed due to better flow mixing induced by the longitudinal swirl flows in the grooved tube.

4.3. Effects of geometric parameters on the thermal-hydraulic performance

4.3.1. Effects of the number of circumferential grooves

Fig. 9 shows the variations of Nusselt number ratios, friction factor ratios and $Q_{*,b}$ values with different numbers of circumferential grooves (N = 4, 6, 8, 10, 12) at P^* = 3. Fig. 9(a) shows that Nusselt number ratios increase with increasing Reynolds number, but the increasing amplitude is quite limited, especially for larger Reynolds numbers. At a given Reynolds number, Nusselt number ratios increase significantly with increasing numbers of circumferential grooves. On the whole, the heat transfer is enhanced by a factor of approximately 1.35–2.17 over those of the smooth tube for various numbers of circumferential grooves. According to Fig. 9(b),

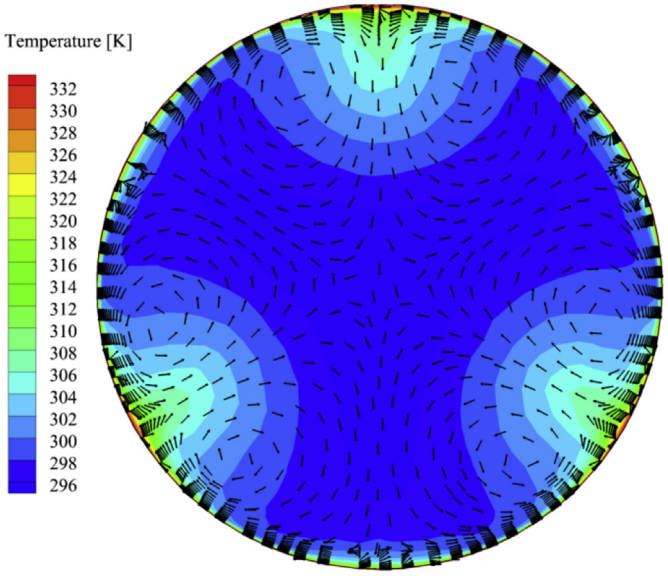

Fig. 8. Tangential velocity vectors and temperature contours in the outlet cross section of the test section at Re = 10170, N = 6 and P^* = 3.

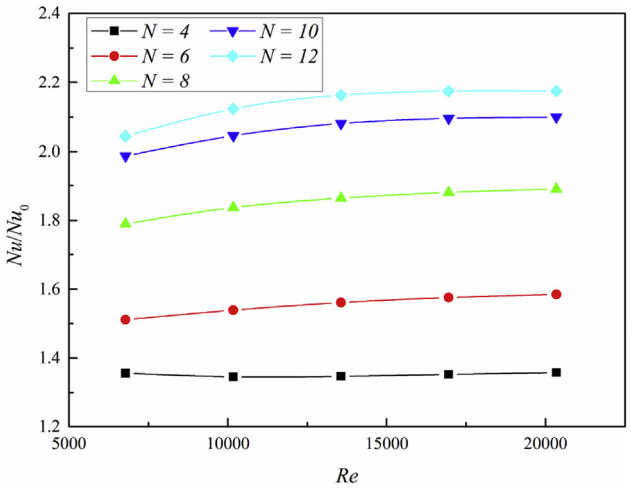

(a)

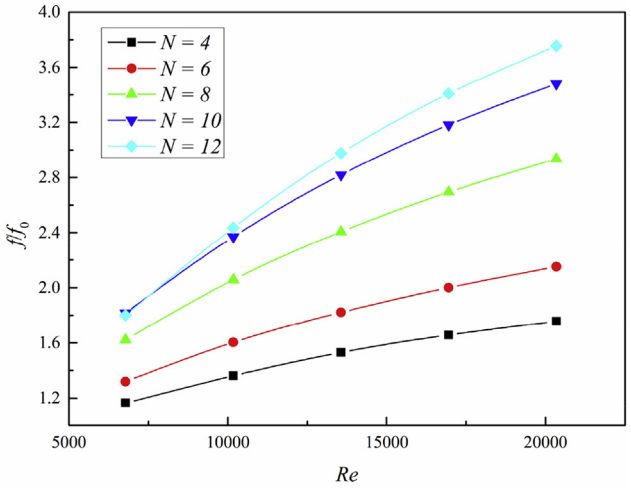

(b)

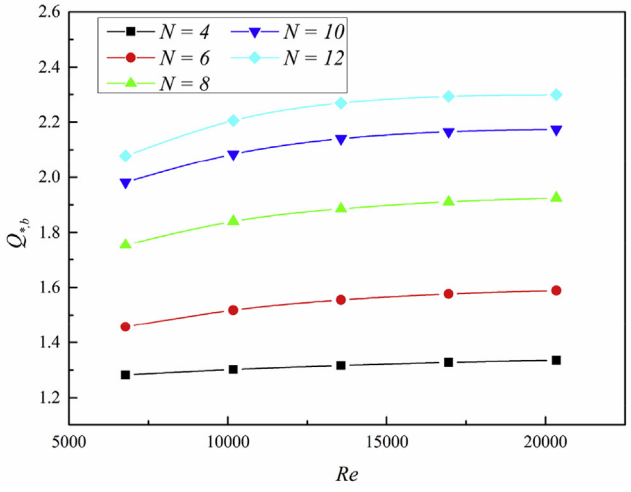

(c)

Fig. 9. Effects of the number of circumferential grooves on flow and heat transfer performance: (a) Nusselt number ratio; (b) friction factor ratio; (c) $Q_{*,b}$.

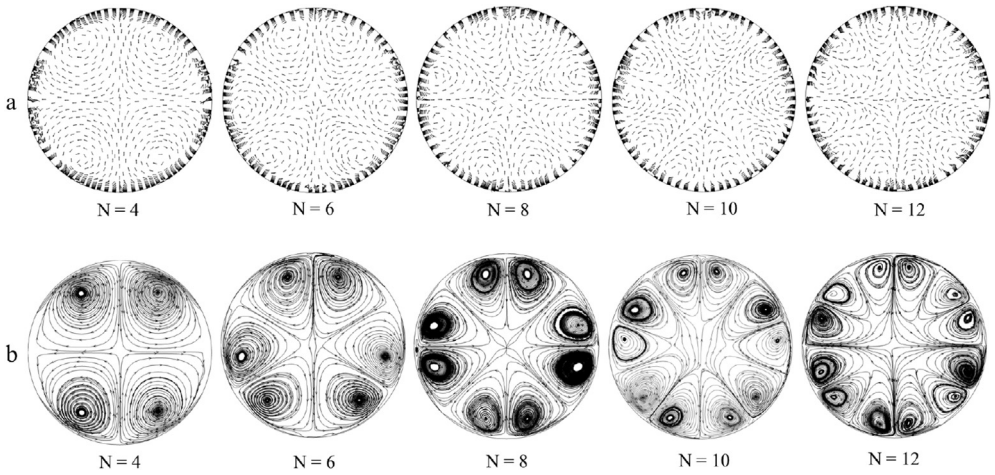

Fig. 10. Tangential velocity vectors and surface streamlines with different numbers of circumferential grooves in the outlet cross section of the test section at *Re* = 10170: (a) tangential velocity vectors; (b) surface streamlines.

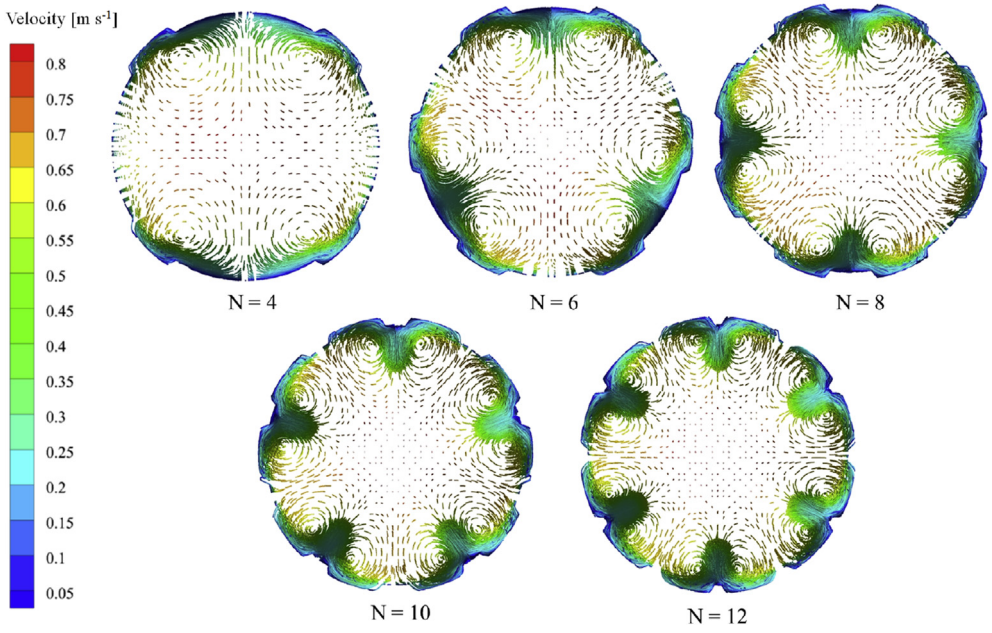

Fig. 11. 3D streamlines in the grooved tubes with different numbers of circumferential grooves at *Re* = 10170.

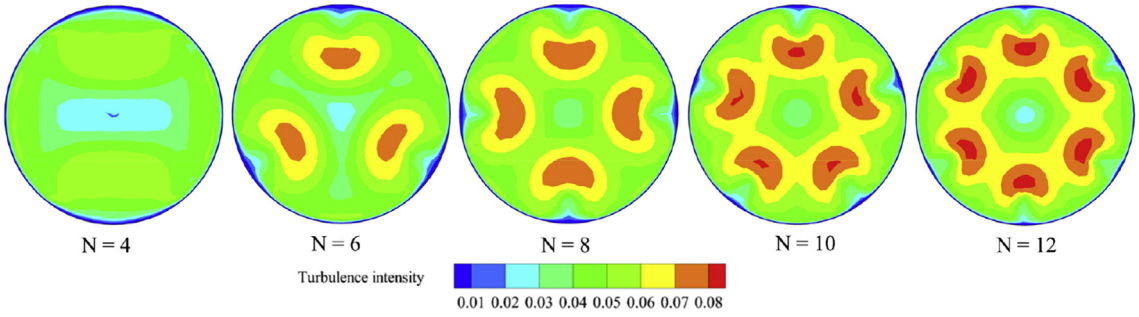

Fig. 12. Turbulence intensity with different numbers of circumferential grooves in the outlet cross section of the test section at *Re* = 10170.

friction factor ratio increases significantly with increasing Reynolds number, which is different from the variation trend of the Nusselt number ratio. At a given Reynolds number, friction factor ratios increase substantially with increasing numbers of circumferential grooves, especially for larger Reynolds numbers. The friction factor is increased by a factor of 1.16–3.75 over those of the smooth tube

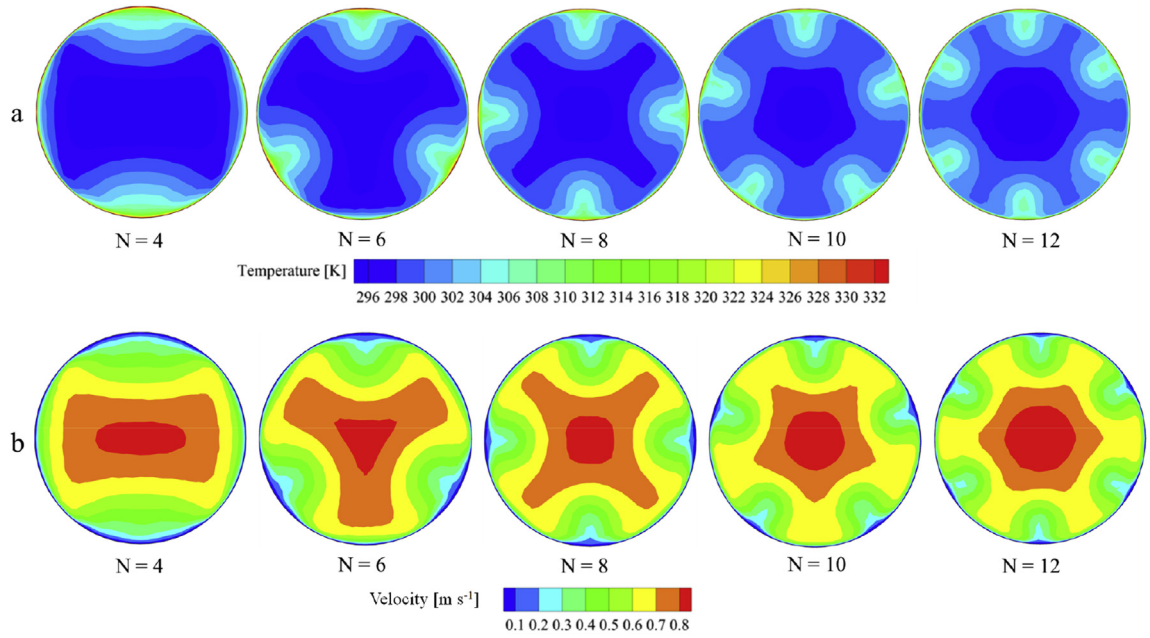

Fig. 13. Temperature and velocity contours with different numbers of circumferential grooves in the outlet cross section of the test section at $Re = 10170$: (a) temperature contours; (b) velocity contours.

for various numbers of circumferential groove.

Fig. 9(c) illustrates the variation of $Q_{*,b}$ values in the grooved tube. The $Q_{*,b}$ values vary from 1.28 to 2.30, which are greater than unity for all the numbers of circumferential grooves, implying that the proposed grooved tube is advantageous over the smooth tube. At a given Reynolds number, the $Q_{*,b}$ values increase with larger N, and the difference for $Q_{*,b}$ values is very small as N increased from 10 to 12, indicating that the increasing space for $Q_{*,b}$ is quite limited with the further increase of N. Therefore, a maximum N of 12 is proposed for applications.

The aforementioned results reveal that the number of circumferential grooves profoundly affect the flow and heat transfer performance in the grooved tube. To analyze the mechanism of the flow and heat transfer, the tangential velocity vectors, surface streamlines, 3D streamlines, turbulence intensity, temperature and velocity contours in the outlet cross section of the test section at $Re = 10170$ are presented in Figs. 10–13.

The tangential velocity vectors and surface streamlines with different numbers of circumferential grooves in the outlet cross section of the test section are shown in Fig. 10. It is apparent that longitudinal swirl flows with multiple vortices are generated due to the existence of discrete inclined grooves, and the number of the induced vortex is proportional to the number of circumferential grooves. It is valuable noting that the area influenced by the vortices is relatively closer to the core flow region at $N = 4$ compared to other numbers of circumferential grooves, and the affected area tend to get closer to the wall with increasing the number of circumferential grooves, which can be attributed to the interaction between the induced vortices. This kind of interaction helps to increase the flow mixing between the core flow and wall regions.

To better present the flow structures in the grooved tubes, 3D streamlines in the grooved tubes with different numbers of circumferential grooves have also been provided, as shown in Fig. 11. It is apparent from the 3D streamlines that multiple longitudinal swirl flows are induced in the grooved tubes, and the number of the longitudinal swirl flows is proportional to the number of circumferential grooves. With the increment of the number of circumferential grooves, the cores of these longitudinal swirl flows are distributed more closely to the wall due to the interaction between the swirl flows. Even though the area affected by single longitudinal swirl flow decreases with more circumferential grooves, the total area affected by all the longitudinal swirl flows increases. Therefore, it can be expected that more fluid in the area affected by longitudinal swirl flows can get better mixed.

The strength of the vortices is characterized in terms of turbulence intensity as illustrated in Fig. 12. It is visible that the turbulence intensity is higher where multiple vortices are generated. Besides, the turbulence intensity increases with increasing numbers of circumferential grooves, indicating that the intensity of flow mixing is enhanced gradually with increasing the number of circumferential grooves. As a result of the intense flow mixing, the temperature is more evenly distributed as shown in Fig. 13 (a). The average temperature increases with increasing numbers of circumferential grooves, which explains why Nusselt number ratios increase significantly with increasing numbers of circumferential grooves. In addition, fluids lose momentum due to flow mixing, resulting in the pressure drop. As shown in Fig. 13(b), the velocity magnitude is smaller where turbulence intensity is high, and the higher the turbulence intensity is, the smaller velocity magnitude is. Therefore, fluids lose more magnitude with increasing number of circumferential grooves, indicating more pressure drop is caused with more grooves. This explains why friction factor ratios increase with increasing numbers of circumferential grooves.

4.3.2. Effects of groove pitch

Variations of Nusselt number ratios, friction factor ratios and $Q_{*,b}$ values with different groove pitch ratios at $N = 12$, $Re = 10170$, are shown in Fig. 14(a), (b) and (c), respectively. Fig. 14(a) shows that Nusselt ratios increase with increasing Reynolds number. But the increasing trend diminishes at elevated Reynolds number, especially for the smaller groove pitch ratio case, like $P^* = 3$. At a given Reynolds number, Nusselt number ratios decrease with increasing groove pitch ratio, implying the use of smaller groove pitch to enhance heat transfer is more effective. For all the groove pitch ratio cases, the heat transfer is enhanced by a factor of

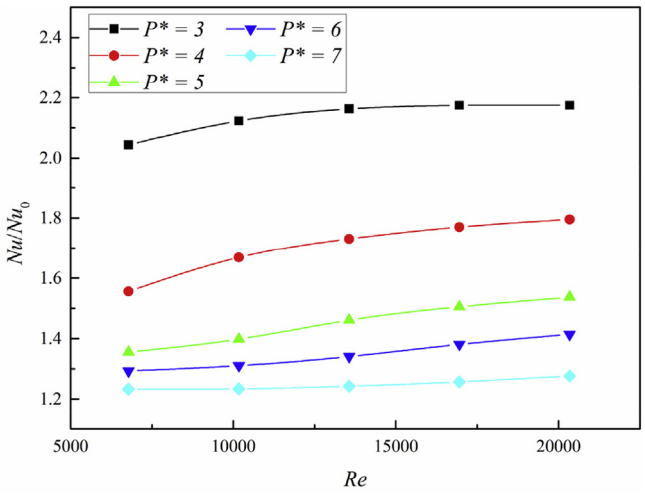

(a)

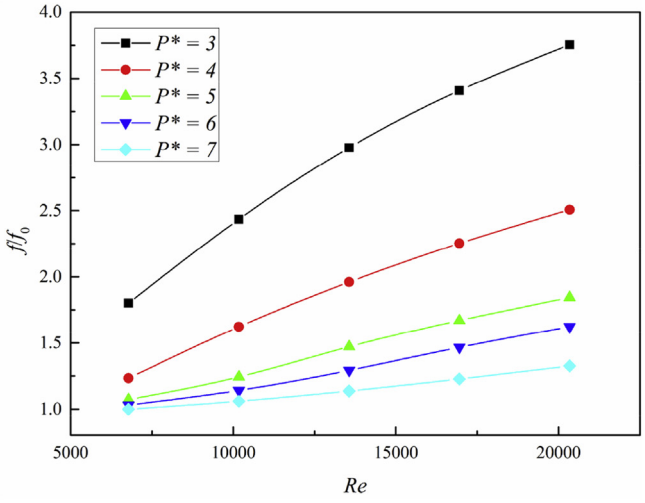

(b)

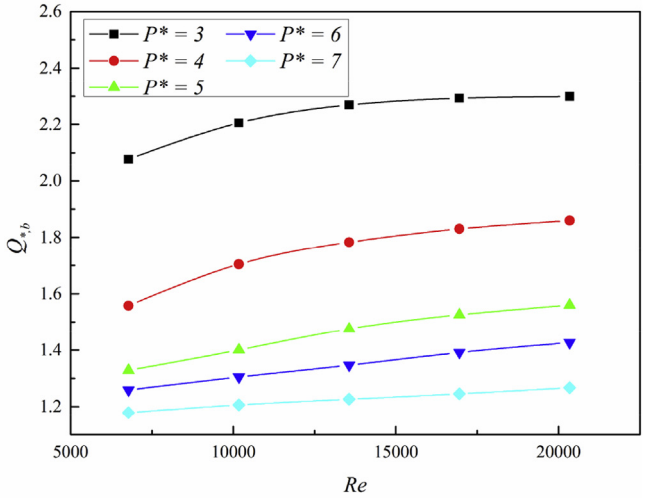

(c)

approximately 1.23–2.17 over those of the smooth tube. Fig. 14(b) illustrates that friction factor ratios increase with increasing Reynolds number, which is consistent with Nusselt number ratios, but the increasing amplitude is much larger than those of Nusselt number ratios. At a given Reynolds number, friction factor ratios decrease with increasing groove pitch ratio. The friction factor is increased by a factor of 1.02–3.75 over those of the smooth tube for all the groove pitch ratio cases.

The effect of groove pitch ratios on is shown in Fig. 14(c). The $Q_{*,b}$ values vary from 1.18 to 2.30 which are above unity for all the cases, and the maximum $Q_{*,b}$ of 2.30 is observed for $P^* = 3$ due to the excellent heat transfer enhancement with relatively low pressure drop. In the case of $P^* = 3$, the actual distance between the grooves is 0.006 m indicating that grooves are very close to each other. Considering the fact the groove length is 0.006 m, the less P^* will lead to the interference between the grooves and thereby impairs the heat transfer performance. Therefore, the smallest pitch ratio of 3 ($P^* = 3$) is recommended for applications.

Fig. 15 shows the local heat flux on the wall at $Re = 10170$, $P^* = 5$. In the present study, heat flux is a reflection of heat transfer performance under constant wall temperature condition. It is noteworthy that the local heat flux is much higher right after the grooves than further downstream from the grooves because strong vortices are induced by the grooves, and the strength of the vortices diminishes with the fluids flowing forward. Therefore, heat transfer enhancement is much higher in the area right after the grooves, and taking advantage of these areas by reducing the groove pitch ratio is an effective way to enhance the overall heat transfer performance. This explains why Nusselt number ratios increase with the decreasing groove pitch ratio. On the other hand, reducing the groove pitch ratio means that the test section has more grooves, and the pressure drop increases consistently with increasing groove number because more flow blockages are created by the grooves, which explains why friction factor ratios increase with decreasing groove pitch ratio.

The analysis above is based on the first law of thermodynamics. To further understand the effects of geometric parameters on the thermal-dynamic performance in the proposed grooved tube and reveal the essence of heat transfer enhancement, it is necessary to perform some analyses based on the second law of thermodynamics, which mainly focuses on the irreversibility caused by the process of heat transfer and flow in the tube. Entropy generation analysis proposed by Bejan [27,28], is a commonly used method to investigate heat transfer performance from the viewpoint of the second law of thermodynamics. Thus, entropy generation analyses are performed in the following section.

4.4. Entropy generation analysis

Taking the grooved tube of length dz as the thermodynamic system, the first and second law of thermodynamic can be expressed as

$$m' dh = q' dz \tag{18}$$

$$dS'_{gen} = m' ds - \frac{q' dz}{T_w} \tag{19}$$

where q' is the heat flux per unit length.

In addition, by using the canonical relation given by

Fig. 14. Effects of groove pitch on flow and heat transfer performance: (a) Nusselt number ratio; (b) friction factor ratio; (c) $Q_{*,b}$.

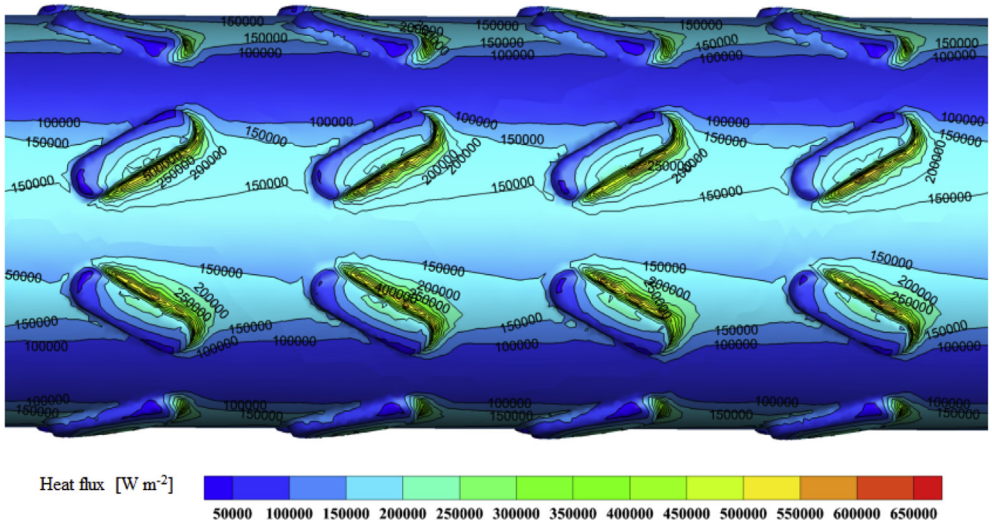

Fig. 15. Local heat flux on the wall at Re = 10170, P^* = 5.

$$Tds = dh - vdp \tag{20}$$

Substituting Eq. (18) and Eq. (20) into Eq. (19) yields the entropy generation rate per length:

$$dS'_{gen} = m' c_p \left[\frac{T_w - T}{TT_w} dT - \frac{1}{\rho c_p T} dP\right] \tag{21}$$

Pressure drop in Eq. (21) is given by

$$dP = -\frac{f\rho u_m}{2D_1} dz \tag{22}$$

The bulk temperature variation of fluid along the grooved tube is given by Sahin [29]:

$$T = T_w - (T_w - T_i)\exp\left[-\frac{4h}{\rho u_m D_1 c_p} z\right] \tag{23}$$

Integrating Eq. (21) along the test section of the grooved tube, total entropy generation is obtained as

$$S'_{gen} = m' c_p \left[\ln\left[\frac{1-\tau e^{-4St\lambda^*}}{1-\tau}\right] - \tau\left(1 - e^{-4St\lambda^*}\right) + \frac{1}{8} f \frac{Ec}{St} \ln\left[\frac{e^{4St\lambda^*} - \tau}{1-\tau}\right]\right] \tag{24}$$

where τ=$(T_w - T_i)/T_w$ is the dimensionless temperature difference, λ^*=L_2/D_1 is the dimensionless length of the test section, $Ec = u_m^2/(c_p T_w)$ is the Eckert number, and St=$h/(\rho u_m c_p)$ is the Stanton number.

To quantize the thermodynamic impact of the augmentation technique, the augmentation entropy generation number proposed by Bejan [27] is defined by

$$N_{s,a} = S'_{gen,a} \Big/ S'_{gen,s} \tag{25}$$

where $S'_{gen,a}$ and $S'_{gen,s}$ are the total entropy generation in the augmented tube and smooth tube, respectively.

When the benefits are evaluated on the basis of first and second law analysis simultaneously, the objectives that should be achieved to receive any profit are $Q_{*,b}$>1 and $N_{s,a}$<1. When several augmented surfaces or techniques are compared the best one is that one with the smallest entropy generation number ratio $N_{s,a}/Q_{*,b}$.

Variation of the entropy generation number ratio $N_{s,a}/Q_{*,b}$ with Reynolds number for different numbers of circumferential grooves is shown in Fig. 16. At a given Reynolds number, the entropy generation number ratio $N_{s,a}/Q_{*,b}$ decreases with increasing the number of circumferential grooves. This indicates that the irreversibility of the heat transfer process is reduced with the increment of circumferential grooves, and more heat can be transferred during the process under the same condition. Therefore, a maximum circumferential groove number of 12 is proposed for applications.

It is valuable noting from Fig. 17 that the entropy generation number ratio $N_{s,a}/Q_{*,b}$ decrease with the reduced groove pitch ratio in all the cases, which implies that decreasing the groove pitch ratio not only enhances the heat transfer, but also reduces the irreversibility of the process. Therefore, the proposed grooved tube is recommended to have a groove pitch ratio of 3 for practical applications.

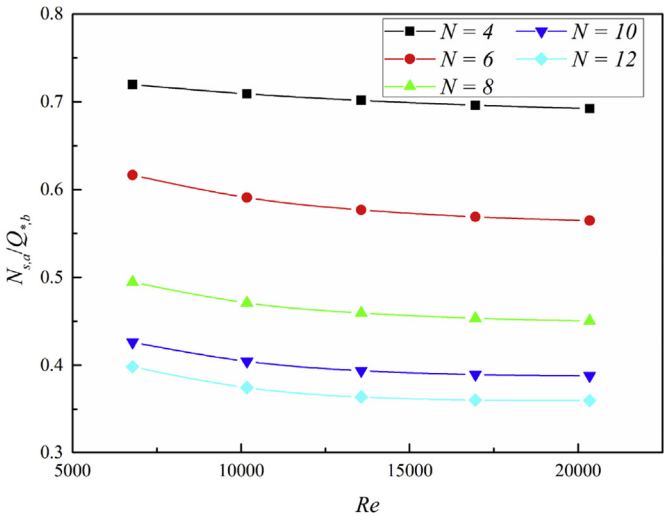

Fig. 16. Variation of the entropy generation number ratio $N_{s,a}/Q_{*,b}$ with Reynolds number for different numbers of circumferential grooves.

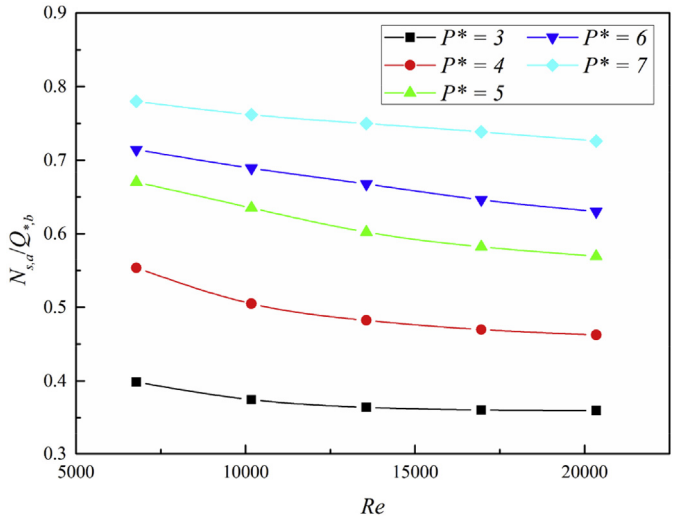

Fig. 17. Variation of the entropy generation number ratio $N_{s,a}/Q_{*,b}$ with Reynolds number for different groove pitch ratios.

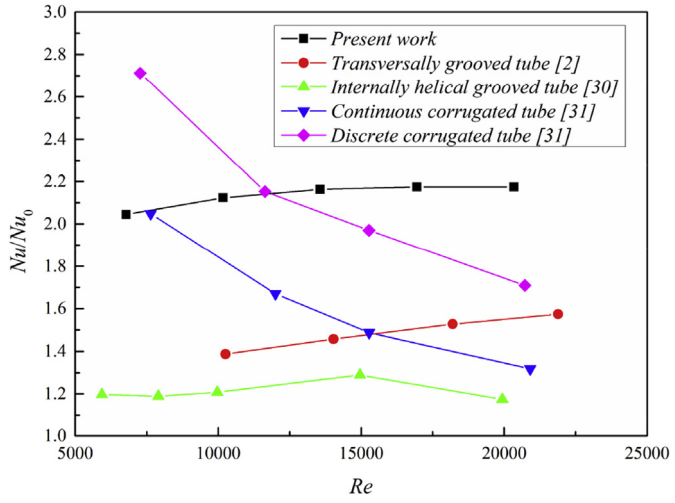

Fig. 18. Comparison with previous work.

4.5. Comparison with previous work

Fig. 18 shows the comparison of the thermal performance between the proposed grooved tube in the present work and some widely used enhanced tubes such as transversally grooved tube [2], internally helical grooved tube [30], continuous corrugated tube [31] and discrete corrugated tube [31]. It is clear that the proposed grooved tube provides considerably higher thermal performance than the transversally grooved tube, internally helical grooved tube and continuous corrugated tube, but lower thermal performance than the discrete corrugated tube at lower Reynolds numbers. The results of the comparison indicate that the proposed grooved tube is very promising for heat transfer enhancement in practical applications. To further improve the overall thermal performance of the grooved tube, more geometric parameters would be investigated and optimized in the future work.

5. Conclusions

Turbulent flow and heat transfer in a circular tube with discrete inclined grooves were numerically investigated. Turbulent flow and heat transfer details, and effects of geometric parameters on the heat transfer performance were presented and analyzed. Entropy generation analyses were performed to further understand the physical mechanism of the enhanced grooved tube. Comparison between the proposed grooved tube and previous enhanced tubes was also conducted. Based on the numerical investigation, following conclusions can be drawn:

(1) Longitudinal swirl flows with multiple vortices are induced in the grooved tube. The flow pattern results in a long flow path and relatively intense flow mixing between the wall and the core flow regions. The temperature is more evenly distributed due to better flow mixing induced by the longitudinal swirl flows.
(2) The number of the induced vortices and the turbulence intensity in the grooved tube increase with increasing numbers of circumferential grooves. For the range of Reynolds numbers investigated, in the tube with discrete inclined grooves, the heat transfer and friction factor are enhanced by a factor of approximately 1.23–2.17 and 1.02 to 3.75 over the smooth tube, respectively. The $Q_{*,b}$ values vary from 1.18 to 2.30 for various numbers of circumferential grooves and groove pitch ratios.
(3) The entropy generation number ratios $N_{s,a}/Q_{*,b}$ decrease with increasing numbers of circumferential grooves and the reduced groove pitch ratio. The proposed grooved tube is recommended to have a number of circumferential grooves of 12 and a groove pitch ratio of 3 for practical applications.
(4) The proposed grooved tube provides considerably higher thermal performance than the transversally grooved tube, internally helical grooved tube and continuous corrugated tube, but lower thermal performance than the discrete corrugated tube at lower Reynolds numbers.

Conflict of interest

None.

Acknowledgments

The work was supported by the National Key Basic Research Program of China (973 Program) (2013CB228302) and the National Natural Science Foundation of China (51376069).

Nomenclature

c_p	specific heat (J kg^{-1} K^{-1})
D_1	inner diameter of the tube (m)
D_2	outer diameter of the tube (m)
Ec	Eckert number
f	friction factor
H	groove depth (m)
h	average heat transfer coefficient (W m^{-2} K^{-1})
k	kinetic energy (m^2 s^{-2})
l	total length of the computation domain (m)
L_1	length of the upstream section (m)
L_2	length of the test section (m)
L_3	length of the downstream section (m)
L	groove length (m)
m	mass flow rate (kg s^{-1})
n	the local coordinate normal to the wall or groove surface
N	number of circumferential groove
Nu	Nusselt number

$N_{s,a}$	entropy generation number
p	pressure (Pa)
Δp	pressure drop (Pa)
P	groove pitch (m)
P^*	groove pitch ratio
Pr	Prandtl number
Q'	total heat flux (W)
q'	heat flux per unit length (W m^{-3})
Re	Reynolds number
St	Stanton number
S'_{gen}	entropy generation rate (W K^{-1})
T	temperature (K)
u_m	mean velocity (m s^{-1})
W	groove width (m)

Greek symbols

α	groove inclination angle (°)
β	expansion coefficient (K^{-1})
ε	dissipation (m^2 s^{-3})
λ	thermal conductivity (W m^{-1} K^{-1})
λ^*	dimensionless length of the test section
μ	dynamic viscosity (Pa s)
ν_t	turbulent eddy viscosity (Pa s)
ρ	density (kg m^{-3})
τ	dimensionless temperature difference
ω	specific dissipation rate (s^{-1})

Subscripts

a	augmented tube
m	mean
i	inlet of the test section
o	outlet of the test section
0	smooth tube
w	wall
f	fluid

References

[1] Sheikholeslami M, Gorji-Bandpy M, Ganji DD. Review of heat transfer enhancement methods: focus on passive methods using swirl flow devices. Renew Sustain Energy Rev 2015;49:444–69.

[2] Bilen K, Cetin M, Gul H, Balta T. The investigation of groove geometry effect on heat transfer for internally grooved tubes. Appl Therm Eng 2009;29(4):753–61.

[3] Aroonrat K, Jumpholkul C, Leelaprachakul R, Dalkilic AS, Mahian O, Wongwises S. Heat transfer and single-phase flow in internally grooved tubes. Int Commun Heat Mass Transf 2013;42:62–8.

[4] Bharadwaj P, Khondge AD, Date AW. Heat transfer and pressure drop in a spirally grooved tube with twisted tape insert. Int J Heat Mass Transf 2009;52(7–8):1938–44.

[5] Lu J, Sheng X, Ding J, Yang J. Transition and turbulent convective heat transfer of molten salt in spirally grooved tube. Exp Therm Fluid Sci 2013;47:180–5.

[6] Lu J, He S, Ding J, Yang J, Liang J. Convective heat transfer of high temperature molten salt in transversely grooved tube. Appl Therm Eng 2013;61(2):157–62.

[7] Goto M, Inoue N, Ishiwatari N. Condensation and evaporation heat transfer of R410A inside internally grooved horizontal tubes. Int J Refrig 2001;24(7):628–38.

[8] Zhang X, Zhang X, Chen Y, Yuan X. Heat transfer characteristics for evaporation of R417A flowing inside horizontal smooth and internally grooved tubes. Energy Convers Manag 2008;49(6):1731–9.

[9] Zhang X, Ji C, Yuan X. Prediction method for evaporation heat transfer of non-azeotropic refrigerant mixtures flowing inside internally grooved tubes. Appl Therm Eng 2008;28(14–15):1974–83.

[10] Zhang X, Zhang J, Ji H, Zhao D. Heat transfer enhancement and pressure drop performance for R417A flow boiling in internally grooved tubes. Energy 2015;86:446–54.

[11] Eiamsa-ard S, Promvonge P. Numerical study on heat transfer of turbulent channel flow over periodic grooves. Int Commun Heat Mass Transf 2008;35(7):844–52.

[12] Eiamsa-ard S, Promvonge P. Thermal characteristics of turbulent rib-grooved channel flows. Int Commun Heat Mass Transf 2009;36(7):705–11.

[13] Bi C, Tang GH, Tao WQ. Heat transfer enhancement in mini-channel heat sinks with dimples and cylindrical grooves. Appl Therm Eng 2013;55(1–2):121–32.

[14] Liu J, Xie G, Simon TW. Turbulent flow and heat transfer enhancement in rectangular channels with novel cylindrical grooves. Int J Heat Mass Transf 2015;81:563–77.

[15] Tang XY, Jiang G, Cao G. Parameters study and analysis of turbulent flow and heat transfer enhancement in narrow channel with discrete grooved structures. Chem Eng Res Des 2015;93:232–50.

[16] Liu W, Liu Z, Jia H, Fan A, Nakayama A. Entransy expression of the second law of thermodynamics and its application to optimization in heat transfer process. Int J Heat Mass Transf 2011;54(13):3049–59.

[17] Jia H, Liu W, Liu Z. Enhancing convective heat transfer based on minimum power consumption principle. Chem Eng Sci 2012;69(1):225–30.

[18] Liu W, Jia H, Liu Z, Fang H, Yang K. The approach of minimum heat consumption and its applications in convective heat transfer optimization. Int J Heat Mass Transf 2013;57(1):389–96.

[19] Jia H, Liu Z, Liu W, Nakayama A. Convective heat transfer optimization based on minimum entransy dissipation in the circular tube. Int J Heat Mass Transf 2014;73:124–9.

[20] Wang J, Liu W, Liu Z. The application of exergy destruction minimization in convective heat transfer optimization. Appl Therm Eng 2015;88:384–90.

[21] Meng J. Enhanced heat transfer technology of longitudinal vortices based on field-coordination principle and its application. Beijing: Power Engineering and Engineering Thermophysics, Tsinghua University; 2003 (In Chinese).

[22] Menter F, Kuntz M, Langtry R. Ten years of industrial experience with the SST turbulence model. Turbul Heat Mass Transf 2003;4(1).

[23] Bergles A, Blumenkrantz A, Taborek J. Performance evaluation criteria for enhanced heat transfer surfaces. In: Proceedings of the 5th international heat transfer conference, vol. 2; 1974. p. 239–43.

[24] Bergles A, Bunn R, Junkhan G. Extended performance evaluation criteria for enhanced heat transfer surfaces. Lett Heat Mass Transf 1974;1:113–20.

[25] Gnielinski V. New equations for heat and mass-transfer in turbulent pipe and channel flow. Int Chem Eng 1976;16(2):359–68.

[26] Petukhov B, Irvine T, Hartnett J. Advances in heat transfer, vol. 6. New York: Academic; 1970. p. 503–4. 6.

[27] Bejan A. Entropy generation through heat and fluid flow. John Wiley & Sons Inc; 1982.

[28] Bejan A. Entropy generation minimization: the method of thermodynamic optimization of finite-size systems and finite-time processes. CRC press; 1995.

[29] Şahin AZ. Entropy generation in turbulent liquid flow through a smooth duct subjected to constant wall temperature. Int J Heat Mass Transf 2000;43(8):1469–78.

[30] Pirbastami S, Moujaes SF, Mol SG. Computational fluid dynamics simulation of heat enhancement in internally helical grooved tubes. Int Commun Heat Mass Transf 2016;73:25–32.

[31] Kathait PS, Patil AK. Thermo-hydraulic performance of a heat exchanger tube with discrete corrugations. Appl Therm Eng 2014;66:162–70.